HHS Public Access

Author manuscript

Differentiation. Author manuscript; available in PMC 2018 December 10.

Published in final edited form as:

Differentiation. 2018 ; 102: 1–9. doi:10.1016/j.diff.2018.05.002.

Epha2 and *Efna5* participate in lens cell pattern-formation

Yuefang Zhou and **Alan Shiels***

Ophthalmology and Visual Sciences, Washington University School of Medicine, St. Louis, MO, USA

Abstract

Ephrin type-A receptor 2 (EPHA2) and one of its ligands, ephrin-A5 (EFNA5), have been associated with loss of eye lens transparency, or cataract, - an important cause of visual impairment. Here we show that mice functionally lacking EPHA2 (*Epha2*-null), EFNA5 (*Efna5*null), or both receptor and ligand (*Epha2/Efna5*-null) consistently develop mostly transparent lenses with an internal refractive disturbance and a grossly disturbed cellular architecture. *In situ* hybridization localized *Epha2* and *Efna5* transcripts to lens epithelial cells and nascent fiber cells at the lens equator. *In vivo* labeling of *Epha2*-null lenses with a thymidine analog detected a significant decrease in lens epithelial cell proliferation within the germinative zone resulting in impaired early lens growth. *Ex vivo* imaging of *Epha2*-null, *Efna5*-null, and *Epha2/Efna5*-null lenses labelled *in vivo* with a membrane-targeted red fluorescent protein revealed misalignment of elongating fiber cells at the lens equator and loss of Y-suture pattern formation near the anterior and posterior poles of the lens. Immuno-fluorescent labeling of lens major intrinsic protein or aquaporin-0 (MIP/AQP0) showed that the precise, radial column patterning of hexagonal fiber cells throughout the cortex region was disrupted in *Epha2*-null, *Efna5*-null and *Epha2/Efna5*-null lenses. Collectively, these data suggest that *Epha2* and *Efna5* participate in the complex, global patterning of lens fiber cells that is necessary for maximal optical quality.

Keywords

Lens; ephrin receptor; ephrin ligand; Y-suture formation; cataract

1. Introduction

Originally discovered in a human erythropoietin-producing hepatoma cell-line, EPH-receptors constitute the largest sub-family (14/58) of mammalian receptor tyrosine kinases (RTKs) that, along with their eph-receptor interacting ligands or ephrins, elicit diverse signaling pathways in embryonic development, adult tissue homeostasis, and various diseases (Lisabeth et al., 2013; Barquilla and Pasquale, 2015; Kania and Klein, 2016). First identified as epithelial cell kinase (ECK), EPH-receptor A2 (EPHA2) belongs to the type-A, EPH-receptor sub-family (EPHA1–8, EPHA10) and like other RTKs, shares a single-pass transmembrane glyco-protein topology with multiple functional domains including a

*Corresponding author: Ophthalmology and Visual Sciences, Box 8096, Washington University School of Medicine, 660 S. Euclid Ave., St. Louis, MO 63110, USA, shiels@vision.wustl.edu (A. Shiels).

cytoplasmic (C-terminal) tyrosine-kinase signaling domain and an extracellular (N-terminal) ligand-binding domain. EPHA2 preferentially binds glycosyl-phosphatidyl-inositol (GPI)-anchored or type-A ephrin ligands (EFNA1–5) and is also referred to as ephrin type-A receptor 2. Canonical EPH-receptor signaling requires direct interaction between EPHA2 and an ephrin-A ligand in neighboring cells (i.e. contact dependent) in order to elicit 'forward' signaling in the receptor-expressing cell and 'reverse' signaling in the ligand-expressing cell. Such bi-directional signaling often results in opposite cellular effects (e.g. adhesion versus repulsion) depending on the specific cellular context (Lisabeth et al., 2013; Barquilla and Pasquale, 2015; Kania and Klein, 2016).

The crystalline lens is a transparent, ellipsoidal, structure located toward the front of the vertebrate eye that plays a central role in anterior eye development and the establishment of normal refractive vision (emmetropia) by facilitating the variable fine-focusing of images onto the photosensitive retina (Beebe and Coats, 2000; Iribarren, 2015; Donaldson et al., 2017). In mammals, the lens develops from a placode of head ectoderm under the influence of a paired box 6 (PAX6)-dependent gene regulatory network and several extracellular signaling pathways to form an exquisitely patterned, cellular structure composed of two cell types enclosed in a collagenous basement membrane or capsule. (Bassnett et al., 2011; Cheng et al., 2017b; Cvekl and Zhang, 2017). The anterior lens surface comprises a monolayer of mitotically competent epithelial cells that terminally differentiate at the lens equator into concentric layers (growthshells) of tightly packed, highly elongated, secondary fiber cells that form the refractive mass of the lens. Lens fiber cell formation is characterized by several unique re-modeling processes including accumulation of crystallins in the cytoplasm, remodeling of the cytoskeleton, specialization of the plasma-membrane, programmed loss of organelles, and formation of a core syncytium (Bassnett et al., 2011; Cheng et al., 2017b; Cvekl and Zhang, 2017). Collectively, these cellular processes are designed to establish and maintain lens transparency, minimize light scattering, and generate a high refractive index.

EPHA2 is a surprisingly abundant component of the lens cell-membrane proteome, where it accounts for approximately 10% of cell signaling molecules (Bassnett et al., 2009). However, the precise role(s) of EPHA2 signaling in lens cell biology remains unclear. Genetic variants in the human EPHA2 gene (*EPHA2*) have been widely associated with clinically heterogeneous forms of inherited pediatric cataract and with acquired or age-related forms of cataract (Shiels et al., 2008; Jun et al., 2009; Bennett et al., 2017; Chen et al., 2017) (https://sites.wustl.edu/catmap). In addition, variants in the human gene for ephrin-A5 (*EFNA5*) have been tentatively associated with age-related cataract (Lin et al., 2014). Lenses of knockout mice that are functionally null for EPHA2 and/or EFNA5 have also been reported to develop a highly variable cataract phenotype with respect to morphology, severity, progression, and penetrance (Cooper et al., 2008; Jun et al., 2009; Cheng and Gong, 2011; Shi et al., 2012; Son et al., 2013; Cheng et al., 2013; Biswas et al., 2016; Cheng et al., 2017a). Here we uncover a consistently abnormal lens cell patterning phenotype in predominantly transparent lenses of mice lacking EPHA2 and/or EFNA5.

2. Materials and methods

2.1. Mice and lenses

Epha2-null mice (Stock no. 006028) (Brantley-Sieders et al., 2004), transgenic tandem-dimer (td)-Tomato (tdT) reporter mice (Stock no. 007576) (Muzumdar et al., 2007), and C57BL/6J (B6J) mice (Stock no. 000664) were obtained from The Jackson Laboratory (Bar Harbor, ME). *Efna5*-null mice (Frisen et al., 1998) were generously provided by Dr. David Feldheim (University of California, Santa Cruz). Absence of EFNA5 protein in lenses of these mice has been confirmed by others (Cooper et al., 2008; Cheng and Gong, 2011; Cheng et al., 2017a). Null mice were genotyped by PCR-amplification as described (Frisen et al., 1998; Shi et al., 2012) and maintained on a predominantly B6J background that lacks a deletion mutation in the gene for lens beaded-filament-structural-protein-2 (CP49) carried by some inbred strains (Simirskii et al., 2006). *Epha2*-null and *Efna5*-null mice were crossed to generate double null (*Epha2/Efna5*-null) mice. Null mice were crossed with tdT-reporter mice (B6J background) to generate null and wild-type littermates that constitutively express membrane-targeted tdT. Expression of tdT was detected *in vivo* by means of a Dual Fluorescent Protein Flashlight (Nightsea, Lexington, MA) and confirmed by PCR-genotyping as described (Muzumdar et al., 2007). Mice were humanely killed by CO_2 asphyxiation followed by cervical dislocation or decapitation. Eyes were removed from age and sex matched littermates and lenses dissected in pre-warmed (37 C) phosphate buffered saline (PBS, #P4417–100TAB, Sigma-Aldrich, St. Louis, MO) then photographed using a dissecting microscope fitted with a digital camera (Stemi 2000; Zeiss, Thornwood, NY). Images were processed with Photoshop Creative Suite 6 (CS6) software (Adobe Systems, San Jose, CA). All mouse procedures were approved by the Institutional Animal Care and Use Committee (IACUC) at Washington University in compliance with the Institute for Laboratory Animal Research (ILAR) guidlines.

2.2. Ex vivo imaging of membrane-localized tdT

Lenses labeled with tdT were positioned in agarose-coated petri-dishes in which a triangular wedge-shape chamber had been cut out then overlaid with pre-warmed cell-culture medium (DMEM/F12 without phenol red, ThermoFisher, Waltham, MA) and imaged using a waterimmersion objective lens attached to a confocal, fluorescence microscope (FluoView FV1000, Olympus, Center Valley, PA) as described (Bassnett and Shi, 2010). Fluorescent images were acquired at various depths (20–400 μm) from the lens surface with the ‘multi-area time-lapse’ function and reassembled into a complete lens image using system-integrated FluoView software.

2.3. In vivo 5-ethynyl-2’deoxyuridine (EdU) labeling

Lens epithelial cell proliferation was measured by labeling S-phase nuclei with the thymidine analog EdU (Invitrogen/ThermoFisher) as described (Bassnett and Shi, 2010; Wiley et al., 2010). Briefly, mice were given an intra-peritoneal (IP) injection of EdU (10 μg/g) one hour before death then dissected lenses were fixed, permeabilized, and labelled using the Click-iT EdU Alexa Fluor 488 Imaging Kit (C10337, ThermoFisher) according to the manufacturers’ instructions. EdU labelled lenses were immobilized in agarose, overlaid with PBS, and imaged as above (2.2). Fluorescent image stacks (500 – 800 μm) of lens

anterior and equatorial quadrants or sectors were acquired (Z-plane) and projected (Y-plane) using system-integrated FluoView software (Olympus). EdU-positive nuclei were counted manually using the count-tool in Photoshop CS6. Hoechst-stained nuclei were counted using MetaMorph software (Molecular Devices, San Jose, CA).

2.4. In situ Hybridization (ISH)

Lens RNA transcripts were localized using the RNAscope 2.0 HD Detection Kit (RED) (P/N 310034) and custom-synthesized oligonucleotide probes to *Epha2* (NM_010139.3, target region 214–1758 bp) and *Efna5* (NM_207654.2, target region 328–987 bp) according to the manufacturers' instructions (Advanced Cell Diagnostics, Inc, Hayward, CA). Briefly, mouse eyes were fixed (24 hr, 20°C) in 10% neutral buffered formalin (Fisher Scientific) and processed using standard formalin-fixed-paraffin-embedded (FFPE) section techniques. Microtome sections (5 μm, RM2255, Leica Microsystems, Buffalo Grove, IL) on glass slides (SuperFrost Plus, ThermoFisher) were baked (1 hr, 60°C), de-waxed in xylene, dehydrated in ethanol, boiled in citrate buffer, then protease treated (10 μg/ml, 40°C, 30 min) in a HybEZ Oven (ACD). Pretreated sections were hybridized with target probes (2 hr, 40°C), followed by signal amplification oligonucleotides (15–30 min, 40°C). For chromogenic labeling, hybridized sections were treated with alkaline phosphatase (AP)-conjugated Fast-Red label probe (15–30 min, 20°C) and FastRed substrate (10 min, 20°C), then counterstained (Gill's Hematoxylin-1/0.01% ammonia-H_2O), mounted (Acrymount, StatLab, McKinney, TX), and imaged under a bright-field microscope fitted with a digital camera (BX61, Olympus, Center Valley, PA).

2.5. Immuno-fluorescence microscopy

Eyes were processed using standard cryo-section or FFPE-section techniques and immunolocalization performed as described (Shi et al., 2012; Zhou et al., 2016). The following primary antibodies were used, anti-EPHA2 (AF639, R&D Systems, Minneapolis, MN), anti-ephrin A5 (38–0400, ThermoFisher), anti-aquaporin 0 (AB3071, EMD Millipore, Billerica, MA). Briefly, for anti-EPHA2 and anti-EFNA5, eyes were fixed (1 hr., 4°C) in 4% paraformaldehyde (16% aqueous solution, #15710, Electron Microscopy Sciences, EMS, Hatfield, PA) diluted in PBS, then cryo-protected by serial incubation in 15% and 30% sucrose/PBS, embedded in TissueTek (EMS) and cryo-sectioned (15 μm) using a cryostat (Cryotome E, ThermoFisher)). Alternatively, for EFNA5 localization, fresh frozen sections were dried, serially fixed (5 min. each) in methanol followed by acetone, and then processed as below with a recombinant mouse EPHA3-Fc chimera protein (#643-A3–200, R&D Systems) that binds to EFNA-ligands (Cooper et al., 2008). For anti-AQP0, eyes were fixed in 4% paraformaldehyde/PBS (16 hr., 4°C), dehydrated, embedded in paraffin, and sectioned (4 μm) using a microtome (RM2255, Leica). Sagittal or coronal eye sections were permeabilized (0.1% Triton X100/PBS 10 min.), blocked (1 hr., 20°C) in Image-iT FX Signal Enhancer (ThermoFisher) then serially incubated with primary antibody (16 hr, 4°C) followed by species-appropriate, Alexa 488-conjugated secondary antibody (1 hr., 20°C), counter-stained with 4,6-Diamidino-2-phenylindole (DAPI, Sigma), and imaged with a confocal microscope (FV1000, Olympus).

2.6 Statistical analysis

Student's t-test was used to determine statistical significance (p) ± standard error.

3. Results

3.1. *Distribution of Epha2* and *Efna5 expression in the lens*

In order to compare the expression pattern of *Epha2* and *Efna5* in the mouse lens we first performed immunofluorescent labeling with antibodies to EPHA2 and EFNA5, and an EPHreceptor-antibody fusion protein (EPHA3-Fc chimera) that binds to EFNA-ligands including EFNA5 (Cooper et al., 2008). EPHA2 antibody decorated radial columns of hexagonal fiber cells throughout the cortex of wild-type lenses but not *Epha2*-null lenses (Supplementary Fig. 1), consistent with immunofluorescent labeling reported previously (Shi et al., 2012). However, neither the EFNA5 antibody nor the EPHA3-Fc chimera produced specific labelling of wild-type lenses that was absent in *Efna5*-null lenses in our hands (data not shown). To confirm expression of *Epha2* and *Efna5* at the transcript level in the wild-type lens we performed ISH using oligo-nucleotide probes. ISH revealed that *Epha2* transcripts were strongly expressed in epithelial cells and peripheral (nascent) fiber cells at the lens equator (Fig. 1A, a) consistent with immunoblotting data reported previously (Shi et al., 2012). Similarly, *Efna5* transcripts were most abundant in the equatorial epithelium and nascent fiber cells; however, the signal intensity appeared to be lower than that of *Epha2* transcripts (Fig. 1B, b). While we cannot confirm colocalized expression at the protein level, our ISH data suggest that *Epha2* and *Efna5* transcripts are co-expressed in the lens epithelium and that both *Epha2* and *Efna5* expression extends into the newly formed fiber cells at the lens equator.

3.2. *Lens optical quality is impaired in Epha2*-null and *Efna5*-null mice

We first compared lens phenotypes of *Epha2*-null, *Efna5*-null, and *Epha2/Efna5*-null mice at post-natal day 21 (P21) under the dissecting microscope. *Epha2*-null lenses appeared grossly transparent (Fig. 2B, C) but were significantly smaller ($p \leq 0.001$) in equatorial diameter (1861.7 ± 3.4 μm, n = 14) than wild-type lenses (1962.7 ± 6.5 μm, n = 8), consistent with our previous studies (Shi et al., 2012). However, unlike wild-type lenses, *Epha2*-null lenses also displayed variable translucent regions of subtle internal refractive disturbance in the absence of frank opacification or cataract (Fig. 2B, C). Similarly, *Efna5*-null lenses appeared grossly transparent and, while similar ($p = 0.388$) in equatorial diameter (1978.5 ± 5.8, n = 8) to wild-type lenses, they also displayed variable translucent regions of internal refractive disturbance in the absence of cataract (Fig. 2D, E). Like *Epha2*-null lenses, *Epha2/Efna5*-null lenses were significantly smaller ($p \leq 0.001$) in equatorial diameter (1853.3 ± 9.3 μm, n = 6) than wild-type lenses. Further, while mostly transparent with variable translucent regions, *Epha2/Efna5*-null lenses also displayed a discrete, superficial anterior polar opacity in approximately half of lenses examined (Fig. 2F). However, *Epha2/Efna5*-null mice did not survive much beyond wean-age (3–4 weeks) preventing further studies of cataract progression.

Since *Epha2*-null lenses were significantly smaller than wild-type lenses, we sought to measure the effects of *Epha2* loss-of-function on lens epithelial cell proliferation and early

lens growth. In order to visualize lens epithelial cell nuclei during the DNA synthesis (S)-phase of the cell-cycle we labelled intact *Epha2*-null and wild-type lenses *in vivo* with the thymidine analog EdU (Fig. 3A). At P8, the number of EdU positive nuclei was significantly lower in *Epha2*-null lenses, particularly within the germinative zone, when compared with wild-type (Fig. 3B, C). The equatorial diameter of *Epha2*-null lenses was also significantly smaller than that of wild-type (Fig. 3D). Overall, these data suggest that *Epha2* plays a positive role in early lens growth and, along with *Efna5*, is required for lens optical quality.

3.3. *Lens suture formation is disturbed in Epha2*-null and *Efna5*-null mice

In order to visualize the internal cellular architecture of intact lenses we generated null and wildtype littermates that constitutively express the red fluorescent protein tdT on cell membranes. First, we focused on the anterior and posterior pole regions of the lens where fiber cell tips converge and overlap to form virtual, Y-shaped (3-branch), suture lines centered on the optical axis (Shi et al., 2012; Kuszak et al., 2004a; Kuszak et al., 2004b). *Ex vivo* imaging of the wildtype-tdT lens pole regions at P7 and P30 revealed Y-shaped, straight suture lines that were rotationally symmetrical (i.e. 120° apart) and centered on the optical axis (Fig. 4A, E, I, M). The anterior suture was larger than the posterior suture and was configured as an upright Y-shape (Fig. 4A, I), whereas, the smaller posterior suture formed an inverted Y-shape (Fig. 4E, M), with respect to the superior-inferior axis of the eye *in vivo* (Shi et al., 2012). By contrast, polar imaging of the *Epha2*-null-tdT, *Efna5*-null-tdT, and *Epha2/Efna5*-null-tdT lenses revealed that neither the anterior nor the posterior sutures were Y-shaped or centered on the optical axis (Fig. 4). At P7, the anterior suture displayed variable branching (≥ 4 branches) of unequal length with no obvious orientation to the posterior suture (Fig. 4B - D). By P30, the anterior suture was profoundly disturbed with no consistent pattern or orientation (Fig. 4J - L). At P7 and P30, the posterior suture was severely disturbed with cohorts of locally aligned fibers targeted away from the optical axis to form offset, ‘cleft-like’ seams with no obvious pattern or orientation (Fig. 4F - H, N - P). These data suggest that, in the lens, *Epha2* and *Efna5* play direct roles in the global targeting of fiber cell ends to form Y-suture patterns at the poles.

3.4. *Lens epithelial-to-fiber cell alignment is disturbed in Epha2*-null and *Efna5*-null mice

We next focused on the lens equator region where anterior epithelial cells undergo terminal differentiation into highly elongated fiber cells that form the crystalline mass of the lens. Ex vivo imaging of wild-type-tdT lenses close to the equatorial surface (10 – 20 μm) revealed the precise alignment of elongating, hexagonal-shaped (in cross-section) fiber cells into meridional rows (Fig. 5A). Such alignment into meridional rows occurs as elongating fiber cells commence migration of their apical ends across the anterior epithelium toward the anterior suture/pole and their basal ends across the posterior capsule toward the posterior suture/pole. Similar equatorial imaging of Epha2-null-tdT, Efna5-null-tdT, and Epha2/Efna5-null-tdT lenses revealed that elongating fiber cells were misaligned, misshapen, or enlarged, and failed to form the meridional rows of hexagons characteristic of wild-type (Fig. 5B - D). At intermediate equatorial depths (100 – 150 μm) in the wild-type-tdT lens, fiber cells were aligned parallel to the anterior-posterior polar or optical axis (Fig. 5E), whereas, in the Epha2-null-tdT, Efna5-null-tdT, and Epha2/Efna5null-tdT lenses fiber cells deviated away from the optical axis particularly near the posterior pole (Fig. 5F - H).

Imaging at greater equatorial depths (350 – 400 μm) in the wild-type-tdT lens revealed the 'fulcrum' (Fig. 5I) where the apical ends of anterior epithelial cells pivot with the apical ends of elongating fiber cells (Sugiyama et al., 2009). In the Epha2-null-tdT lens, fulcrum formation was disturbed showing an irregular interface, with multiple focal points, compared to the well-defined, continuous interface of wild-type (Fig. 5I, J). In the Efna5-null-tdT lens, while the fulcrum appeared less disturbed than that in the Epha2-null-tdT lens, abnormally shaped and oriented elongating epithelial cells were present (Fig. 5K). However in the Epha2/Efna5null-tdT lens, fulcrum formation was grossly disturbed with many abnormally shaped and enlarged elongating epithelial cells (Fig. 5L). These data suggest that Epha2 and Efna5 play direct roles in epithelial-to-fiber cell alignment and fulcrum pattern-formation at the lens equator.

3.5 *Lens radial cell column formation is disturbed Epha2*-null and *Efna5*-null mice

In order to visualize the radial organization and integrity of lens fiber cell membranes we performed immuno-fluorescent labelling of fixed eye sections using an antibody to lens major intrinsic protein or aquaporin-0 (MIP/AQP0) (Bassnett et al., 2009). In the wild-type lens, antiAQP0 labeling revealed characteristic radial columns of flattened hexagonal fiber cells of similar cross-sectional area serially aligned throughout the cortical region (Fig. 6A - C) (Kuszak et al., 2004a). By contrast, in the *Epha2-null* lens anti-AQP0 labeling revealed that the radial patterning of fiber cells was profoundly disorganized, particularly in the inner cortex (Fig. 6D - F). Instead of flattened hexagons, most *Epha2-null* fiber cells exhibited an irregular crosssectional size and shape, often pentagonal, and were randomly arranged throughout the cortex. Similarly, in *Efna5-null* and *Epha2/Efna5*-null lenses anti-AQP0 labeling highlighted disorganization of radial cell patterning, particularly in the inner cortex, with many enlarged cells present in the latter (Fig. 6G - L). These data suggest that while fiber cell membrane integrity was maintained in the *Epha2-null*, *Efna5-null*, and *Epha2/Efna5*-null lenses, the radial column patterning of hexagonal fiber cells was disturbed.

4. Discussion

In this study, we have demonstrated that mice functionally null for *Epha2* or *Efna5* consistently developed grossly transparent lenses with degraded optical quality in the absence of cataract. While mostly transparent, lenses doubly null for *Epha2* and *Efna5* were also optically degraded and, in addition, exhibited a discrete, superficial anterior polar cataract in ~50% of lenses. At the cellular level, disruption of *Epha2* resulted in reduced proliferation of lens epithelial-cells in the germinative zone and gross disorganization of lens fiber-cell architecture. *Ex vivo* imaging and immuno-localization revealed that *Epha2* was required for; 1) alignment of elongating fiber-cells into meridional rows and formation of the fulcrum at the lens equator, 2) formation of Y-sutures centered on the anterior-posterior polar axis of the lens and, 3) radial column formation of hexagonal fiber-cells throughout the lens cortex. Similarly, *Efna5-null* lenses and those doubly null for *Epha2* and *Efna5* consistently displayed disturbed meridional row patterns at the equator, disturbed radial cell column patterns throughout the cortex, and disturbed suture patterns at the poles. Collectively, our data suggest that *Epha2* and *Efna5* participate in the complex, global patterning of lens fiber cells necessary for maximal optical quality.

Disruption of *Epha2* or *Efna5*, located on mouse chromosomes 4 and 17 respectively, has been reported to exert dramatically variable effects on lens phenotype. Two *Epha2*-null mouse strains generated by gene-trapping strategies, on either a predominantly FVB/NJ or C57Bl/6 genetic background, have been reported to develop a progressive cortical cataract phenotype with incomplete penetrance (~ 80% by 12 months of age) that culminates in total cataract and lens rupture by 6 – 8 months of age (Jun et al., 2009). Similarly, *Efna5*-null mice generated by homologous recombination on a mixed (C57BL/6;S129;CD-1) genetic background developed dense nuclear cataract with incomplete penetrance (~ 87% by 6 months of age) that usually manifest by P21 and then progressed in severe cases to total lens disruption (Cooper et al., 2008; Son et al., 2013; Biswas et al., 2016). In stark contrast, *Epha2*-null and *Efna5*-null mice generated by homologous recombination on a predominantly C57BL/6J background were reported to display a much less severe cataract phenotype characterized by mild nuclear opacities or mild anterior polar opacities, respectively, with incomplete penetrance (Cheng and Gong, 2011; Cheng et al., 2013; Cheng et al., 2017a). Recently, lenses of mice doubly null for *Epha2* and *Efna5* on the B6J background were reported to develop an 'additive phenotype' combining the mild nuclear cataract in *Epha2*-null lenses with the mild anterior-polar cataract in *Efna5*-null lenses (Cheng et al., 2017a). Conversely, we have not found cataract in either *Epha2*-null or *Efna5*-null lenses generated by homologous recombination on the B6J background. However, we did observe anterior polar cataract in ~50% of *Epha2/Efna5*-null lenses (Fig. 2). While we cannot account specifically for cataract heterogeneity in lenses from *Epha2*-null and/or *Efna5*-null mice, it is likely that the gene-targeting method and genetic background modifier effects combine to influence cataract phenotype. In addition, environmental factors may contribute to lens phenotype since cataract penetrance in *Epha2*-null mice was reported to increase from ~80% to 100% after treatment with a skin carcinogen (Jun et al., 2009). These observations suggest that breeding of *Epha2*-null or *Efna5*-null alleles onto different genetic backgrounds, in combination with exposure to a known environmental risk factor (e.g. UV-radiation), may facilitate genetic mapping and identification of modifier genes that influence susceptibility to age-related cataract.

Beyond cataract phenotype, our imaging studies of *Epha2*-null and/or *Efna5*-null lenses, labelled with membrane-targeted tdT, lead us to speculate that Y-suture malformation at the lens poles and disturbed radial hexagonal-cell columns within the lens cortex may result from misaligned meridional rows of hexagonal cells and fulcrum disturbance at the lens equator (Fig. 4 – 6). Thus, we further speculate that early patterning defects in lens cell differentiation at the equator (meridional row/fulcrum malformation) may contribute to patterning defects later in lens cell differentiation and maturation in the cortex and at the poles (radial column/suture malformation). By contrast, Y-suture formation was reported to be normal in *Epha2*-null lenses labelled with green fluorescent protein (GFP) despite the presence of misaligned meridional rows of non-hexagonal fiber cells and disturbed fulcrum formation at the lens equator (Cheng and Gong, 2011; Cheng et al., 2013; Cheng et al., 2017a). Discrepancies in image resolution between uniform tdT labeling of cell membranes versus mosaic GFP labeling of cytoplasm may account, in part, for conflicting interpretations of lens suture organization. Nevertheless, computer assisted modeling has shown that Y-suture formation results from an intricate patterning of secondary fiber cells

with variable shapes and lengths (Kuszak et al., 2004b). Characteristic of Y-suture formation is the S-shaped or opposite-end curvature of fiber cells that results in their anterior ends paring with a defined set of fiber cells at the anterior suture branches (upright-Y) that are different to those at the posterior suture branches (inverted-Y). In humans and other primates, Y-suture formation during gestation is overlaid after birth by the progressively more complex branching pattern of star sutures that is believed to enhance the optical quality and fine-focusing ability, or accommodation, of the adult lens (Kuszak et al., 2004b). Our imaging data from null lenses labelled with tdT suggest, for the first time, that both *Epha2* and *Efna5* are critical for Y-suture pattern formation at the lens poles. Further, we speculate that the more complex star-suture patterning found in human lenses may contribute to the clinical heterogeneity of inherited and age-related forms of cataract associated with pathogenic mutations or deleterious variants in *EPHA2*, respectively (Shiels et al., 2008; Jun et al., 2009; Bennett et al., 2017; Chen et al., 2017).

While suture pattern formation reflects the complex, global, fiber cell architecture of the lens, relatively little is known about the molecular mechanisms controlling this cell patterning process. The grossly disturbed suture formation in the *Epha2*-null and *Efna5*-null lenses reported here, along with other fiber cell malformations (loss of meridional rows, fulcrum integrity, and radial hexagonal-cell columns) strongly suggest that EPHA2-dependent signaling participates in lens fiber-cell pattern-formation. Currently, the identity of EPHA2 ligands in the lens remains controversial with at least two ephrin type-A ligands, EFNA5 and EFNA1, proposed (Cooper et al., 2008; Jun et al., 2009). However, interaction between EPHA2 and EFNA5 has been disputed largely based on an additive cataract phenotype observed in lenses lacking both EPHA2 and EFNA5 (Cheng et al., 2017a). While we cannot directly confirm or refute canonical receptor-ligand interaction between EPHA2 and EFNA5 in the lens, the overlapping ISH pattern of lens *Epha2* and *Efna5* transcripts (Fig. 1) suggest that EPHA2 and EFNA5 are co-expressed in epithelial cells and nascent fiber cells at the lens equator. Regardless of ligand, EPHA2ephrin interaction has been implicated in at least three different signaling pathways that are important in the lens. First, EPHA2-EFNA5 interaction has been associated with regulation of the adherens junction complex involved in lens fiber cell packing (Cooper et al., 2008). Second, EPHA2-ephrin interaction has been proposed to activate Src kinase signaling in order to regulate fiber cell alignment and fulcrum formation at the lens equator (Cheng et al., 2013). Finally, EPHA2-ephrin interaction was reported to engage in crosstalk with fibroblast growth factor receptor (FGFR)-signaling, the primary growth factor pathway involved in lens development and fiber cell differentiation (Lee et al., 2016). Functional interaction between EPHA and FGF receptors has also been reported outside the lens (Sawada et al., 2015). Currently, we are investigating which of these candidate pathways are important for the lens growth inhibition and fiber cell patterning defects communicated here.

Supplementary Material

Refer to Web version on PubMed Central for supplementary material.

Acknowledgements

We thank T. Bennett for technical support and B. McMahan and G. Ling for histology support. This work was supported by NIH/NEI grants EY023549 (to A.S.) and EY02687 (Core Grant for Vision Research) and an unrestricted grant to the Department of Ophthalmology and Visual Sciences from Research to Prevent Blindness (RPB).

Abbreviations:

EPH	erythropoietin producing hepatocellular-carcinoma
EPHA2	EPH receptor A2 or ephrin type-A receptor 2 protein symbol
EFNA5	ephrin-A5 protein symbol
Epha2	mouse EPHA2 gene symbol
Efna5	mouse ephrin-A5 gene symbol
EdU	5-ethynyl2'deoxyuridine
ISH	*in situ* hybridization
tdT	tandem-dimer Tomato
DAPI	4,6-Diamidino-2phenylindole
MIP/AQP0	major intrinsic protein/aquaporin-0

References

Barquilla A, Pasquale EB, 2015 Eph receptors and ephrins: therapeutic opportunities. Ann. Rev. Pharmacol. Toxicol 55, 465–487. [PubMed: 25292427]

Bassnett S, Shi Y, 2010 A method for determining cell number in the undisturbed epithelium of the mouse lens. Mol. Vis 16, 2294–2300. [PubMed: 21139698]

Bassnett S, Shi Y, Vrensen GF, 2011 Biological glass: structural determinants of eye lens transparency. Philos. Trans. R. Soc. Lond. B Biol. Sci 366, 1250–1264. [PubMed: 21402584]

Bassnett S, Wilmarth PA, David LL, 2009 The membrane proteome of the mouse lens fiber cell. Mol. Vis 15, 2448–2463. [PubMed: 19956408]

Beebe DC, Coats JM, 2000 The lens organizes the anterior segment: specification of neural crest cell differentiation in the avian eye. Dev. Biol 220, 424–431. [PubMed: 10753528]

Bennett TM, M'Hamdi O, Hejtmancik JF, Shiels A, 2017 Germ-line and somatic EPHA2 coding variants in lens aging and cataract. PLoS One 12, e0189881. [PubMed: 29267365]

Biswas S, Son A, Yu Q, Zhou R, Lo WK, 2016 Breakdown of interlocking domains may contribute to formation of membranous globules and lens opacity in ephrin-A5(−/−) mice. Exp. Eye Res 145, 130–139. [PubMed: 26643403]

Brantley-Sieders DM, Caughron J, Hicks D, Pozzi A, Ruiz JC, Chen J, 2004 EphA2 receptor tyrosine kinase regulates endothelial cell migration and vascular assembly through phosphoinositide 3-kinase-mediated Rac1 GTPase activation. J. Cell Sci 117, 2037–2049. [PubMed: 15054110]

Chen J, Wang Q, Cabrera PE, Zhong Z, Sun W, Jiao X, Chen Y, Govindarajan G, Naeem MA, Khan SN, Ali MH, Assir MZ, Rahman FU, Qazi ZA, Riazuddin S, Akram J, Riazuddin SA, Hejtmancik JF, 2017 Molecular Genetic Analysis of Pakistani Families With Autosomal Recessive Congenital Cataracts by Homozygosity Screening. Invest. Ophthalmol. Vis. Sci 58, 2207–2217. [PubMed: 28418495]

Cheng C, Ansari MM, Cooper JA, Gong X, 2013 EphA2 and Src regulate equatorial cell morphogenesis during lens development. Development 140, 4237–4245. [PubMed: 24026120]

Cheng C, Fowler VM, Gong X, 2017a EphA2 and ephrin-A5 are not a receptor-ligand pair in the ocular lens. Exp. Eye Res 162, 9–17. [PubMed: 28648759]

Cheng C, Gong X, 2011 Diverse roles of Eph/ephrin signaling in the mouse lens. PLoS One 6, e28147. [PubMed: 22140528]

Cheng C, Nowak RB, Fowler VM, 2017b The lens actin filament cytoskeleton: Diverse structures for complex functions. Exp. Eye Res 156, 58–71. [PubMed: 26971460]

Cooper MA, Son AI, Komlos D, Sun Y, Kleiman NJ, Zhou R, 2008 Loss of ephrin-A5 function disrupts lens fiber cell packing and leads to cataract. Proc. Natl. Acad. Sci. U.S.A 105, 16620–16625. [PubMed: 18948590]

Cvekl A, Zhang X, 2017 Signaling and Gene Regulatory Networks in Mammalian Lens Development. Trends Genet 33, 677–702. [PubMed: 28867048]

Donaldson PJ, Grey AC, Maceo Heilman B., Lim JC, Vaghefi E, 2017 The physiological optics of the lens. Prog. Retin. Eye Res 56, e1–e24. [PubMed: 27639549]

Frisen J, Yates PA, McLaughlin T, Friedman GC, O'Leary DD, Barbacid M, 1998 Ephrin-A5 (AL-1/RAGS) is essential for proper retinal axon guidance and topographic mapping in the mammalian visual system. Neuron 20, 235–243. [PubMed: 9491985]

Iribarren R, 2015 Crystalline lens and refractive development. Prog Retin Eye Res 47, 86–106. [PubMed: 25683786]

Jun G, Guo H, Klein BE, Klein R, Wang JJ, Mitchell P, Miao H, Lee KE, Joshi T, Buck M, Chugha P, Bardenstein D, Klein AP, Bailey-Wilson JE, Gong X, Spector TD, Andrew T, Hammond CJ, Elston RC, Iyengar SK, Wang B, 2009 EPHA2 is associated with age-related cortical cataract in mice and humans. PLoS Genet 5, e1000584. [PubMed: 19649315]

Kania A, Klein R, 2016 Mechanisms of ephrin-Eph signalling in development, physiology and disease. Nature reviews. Mol. Cell Biol 17, 240–256.

Kuszak JR, Zoltoski RK, Sivertson C, 2004a Fibre cell organization in crystalline lenses. Exp. Eye Res 78, 673–687. [PubMed: 15106947]

Kuszak JR, Zoltoski RK, Tiedemann CE, 2004b Development of lens sutures. Int. J. Dev. Biol 48, 889–902. [PubMed: 15558480]

Lee S, Shatadal S, Griep AE, 2016 Dlg-1 Interacts With and Regulates the Activities of Fibroblast Growth Factor Receptors and EphA2 in the Mouse Lens. Invest. Ophthalmol. Vis. Sci 57, 707–718. [PubMed: 26906157]

Lin Q, Zhou N, Zhang N, Qi Y, 2014 Mutational screening of EFNA5 in Chinese agerelated cataract patients. Ophthalmic Res 52, 124–129. [PubMed: 25300504]

Lisabeth EM, Falivelli G, Pasquale EB, 2013 Eph receptor signaling and ephrins. Cold Spring Harb. Perspect. Biol 5.

Muzumdar MD, Tasic B, Miyamichi K, Li L, Luo L, 2007 A global double-fluorescent Cre reporter mouse. Genesis 45, 593–605. [PubMed: 17868096]

Sawada T, Arai D, Jing X, Furushima K, Chen Q, Kawakami K, Yokote H, Miyajima M, Sakaguchi K, 2015 Trans-Activation between EphA and FGFR Regulates Self-Renewal and Differentiation of Mouse Embryonic Neural Stem/Progenitor Cells via Differential Activation of FRS2α. PLoS One 10, e0128826. [PubMed: 26024354]

Shi Y, De Maria A, Bennett T, Shiels A, Bassnett S, 2012 A role for epha2 in cell migration and refractive organization of the ocular lens. Invest. Ophthalmol. Vis. Sci 53, 551559.

Shiels A, Bennett TM, Knopf HL, Maraini G, Li A, Jiao X, Hejtmancik JF, 2008 The EPHA2 gene is associated with cataracts linked to chromosome 1p. Mol. Vis 14, 2042–2055. [PubMed: 19005574]

Simirskii VN, Lee RS, Wawrousek EF, Duncan MK, 2006 Inbred FVB/N mice are mutant at the cp49/Bfsp2 locus and lack beaded filament proteins in the lens. Invest. Ophthalmol. Vis. Sci 47, 4931–4934. [PubMed: 17065509]

Son AI, Cooper MA, Sheleg M, Sun Y, Kleiman NJ, Zhou R, 2013 Further analysis of the lens of ephrin-A5−/− mice: development of postnatal defects. Mol. Vis 19, 254–266. [PubMed: 23401654]

Sugiyama Y, Akimoto K, Robinson ML, Ohno S, Quinlan RA, 2009 A cell polarity protein aPKClambda is required for eye lens formation and growth. Dev. Biol 336, 246–256. [PubMed: 19835853]

Wiley LA, Shui YB, Beebe DC, 2010 Visualizing lens epithelial cell proliferation in whole lenses. Mol. Vis 16, 1253–1259. [PubMed: 20664699]

Zhou Y, Bennett TM, Shiels A, 2016 Lens ER-stress response during cataract development in Mip-mutant mice. Biochim. Biophys. Acta 1862, 1433–1442. [PubMed: 27155571]

Highlights

- EPHA2 and EFNA5 transcripts co-localize in the lens
- EPHA2 and EFNA5 enhance lens optical quality
- EPHA2 and EFNA5 facilitate Y-suture formation at the lens poles
- EPHA2 and EFNA5 facilitate radial cell column formation within the lens cortex
- EPHA2 and EFNA5 facilitate epithelial-to-fiber cell alignment at the lens equator

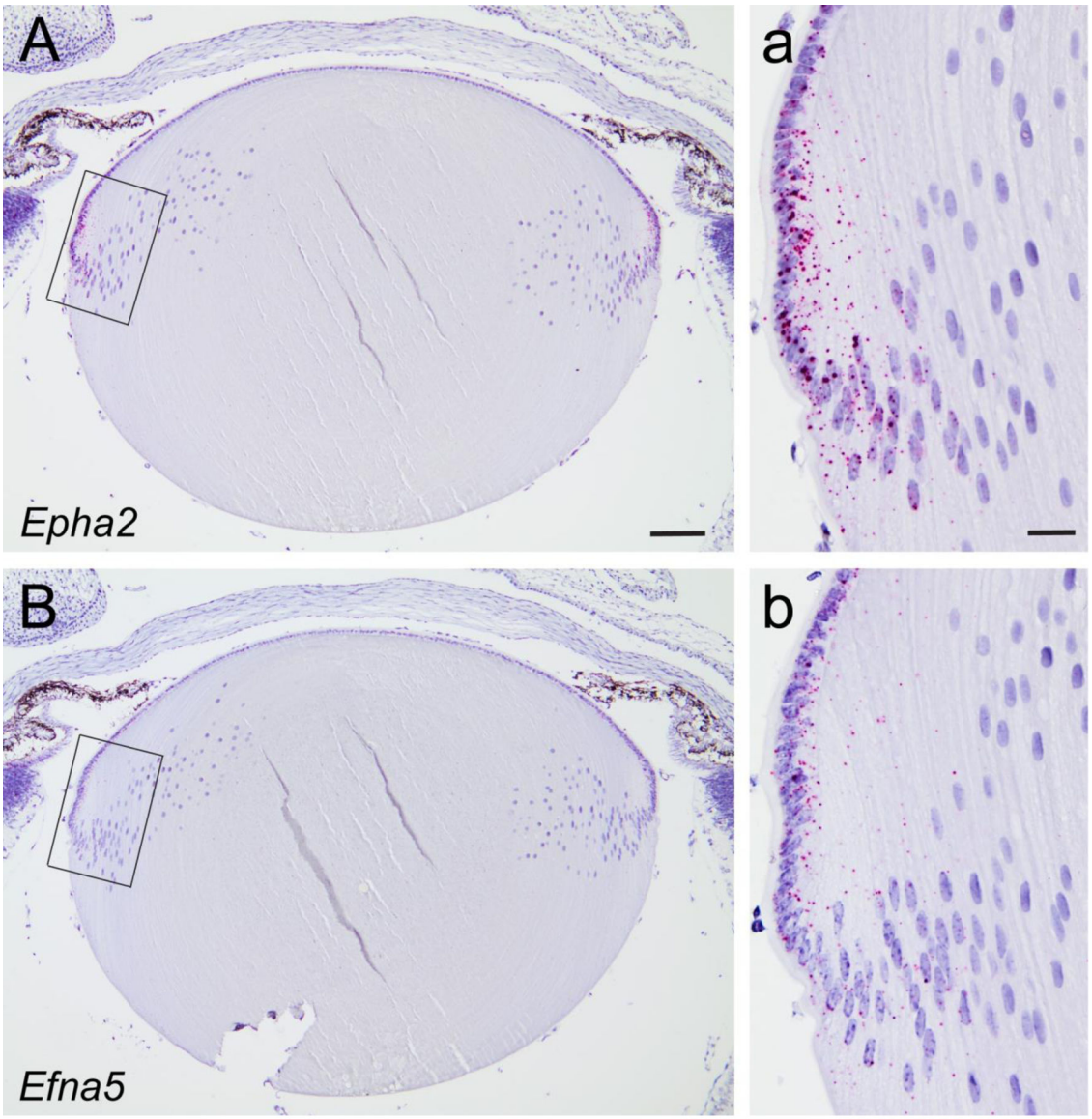

Fig. 1.

In situ hybridization of *Epha2* and *Efna5* transcripts in the mouse lens. (**A, B**) Chromogenic labeling (red dots) of *Epha2* (**A, inset a**) and *Efna5* (**B, inset b**) transcripts in the mouse lens (P3) showing that both transcripts were localized to the equatorial epithelium and nascent fiber cells. Cell nuclei were counter-stained with hematoxylin (blue). Scale bar: 100 μm (A, B), 20 μm (a, b).

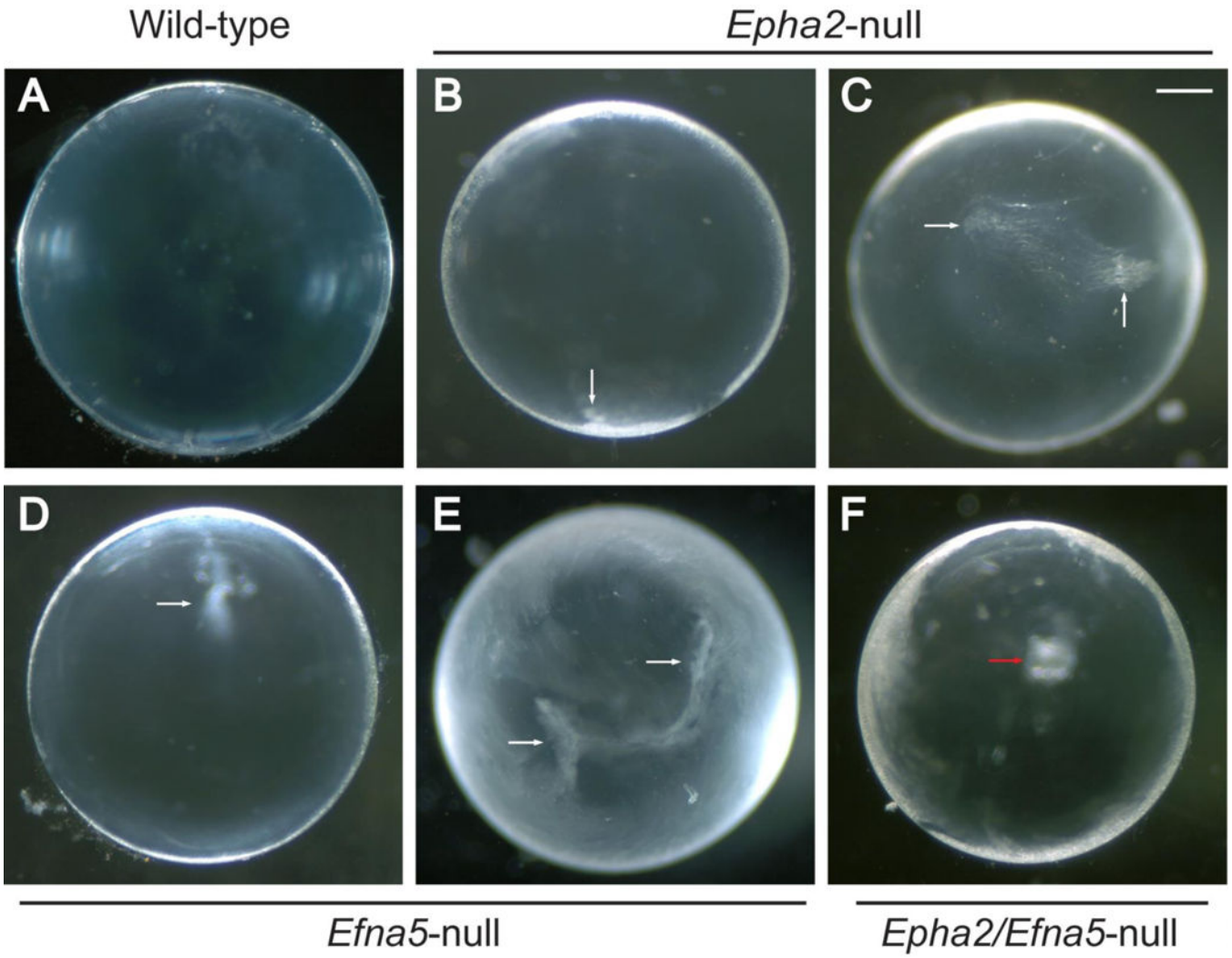

Fig. 2.

Dissecting microscope images of the *Epha2*-null, *Efna5*-null, and *Epha2/Efna5*-null mouse lens phenotypes (P21). (**A-F**) Anterior-pole view of wild-type (**A**), *Epha2*-null (**B, C**), *Efna5*-null (**D, E**), and *Epha2/Efna5*-null (**F**) lenses under dark-field illumination. *Epha2*-null lenses (**B, C**) and *Efna5*-null lenses (**D, E**) exhibited variable translucent regions of internal refractive disturbance (white arrows) while mostly transparent. *Epha2/Efna5*-null lenses (**F**) were also mostly transparent but also exhibited anterior polar opacities in ~50% of cases (red arrow). Scale bar: 300 μm. (n = 18, 14, 8, and 8 for wild-type, *Epha2*-null, *Efna5*-null, and *Epha2/Efna5*-null lenses, respectively, with representative images shown).

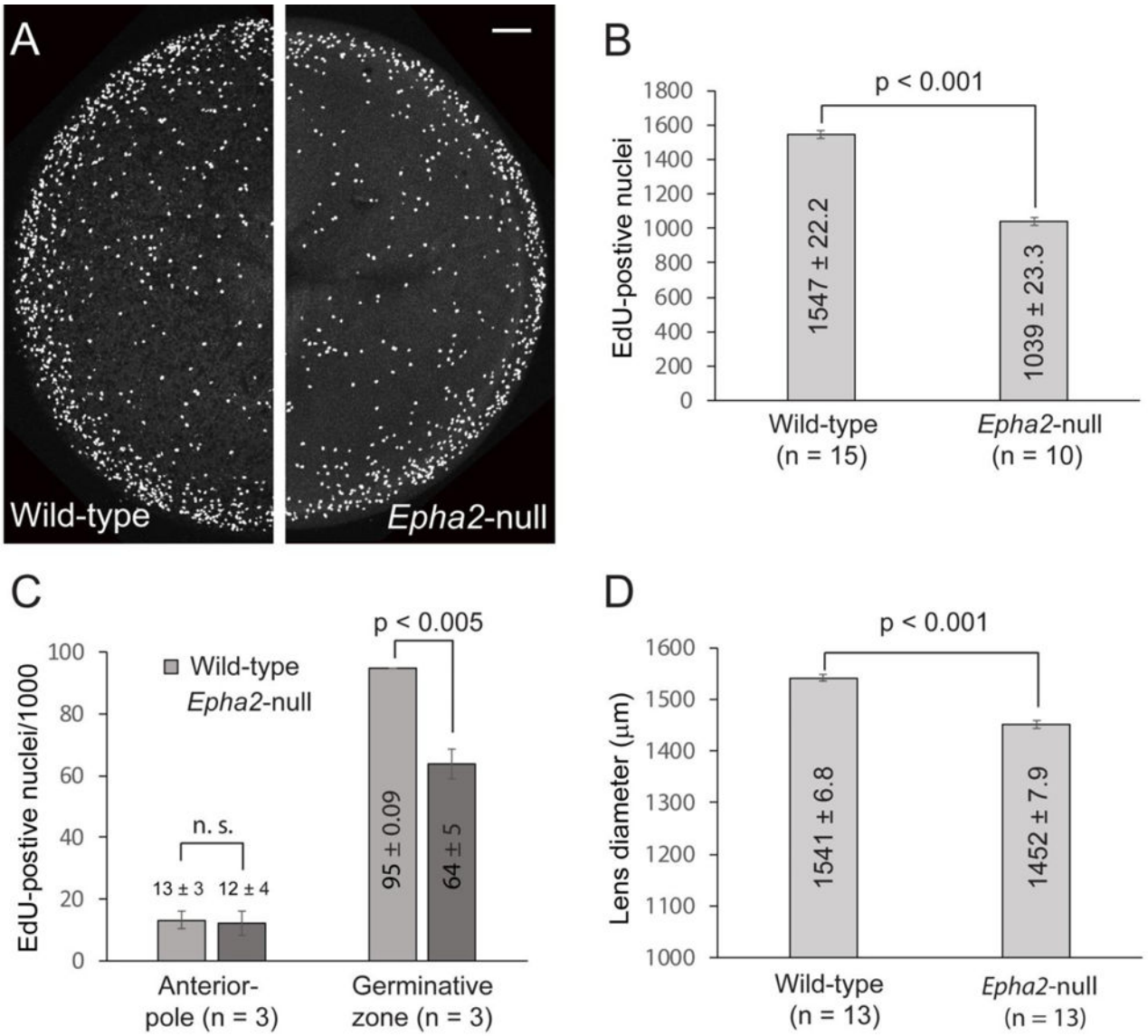

Fig. 3.

Fluorescence imaging of S-phase epithelial cell nuclei in the mouse lens (P8). (**A**) EdU labeling of intact wild-type (left panel) and *Epha2*-null (right panel) lenses showing the increased concentration of S-phase cell nuclei in the germinative zone at the lens equator (outer) compared with the anterior pole region (central). Scale bar: 100 μm. (**B, C**) Both the raw global count (**B**) and the normalized count/1000 nuclei (**C**) of EdU-positive nuclei in the *Epha2*-null lens were significantly less than wild-type. (**D**) The equatorial dimeter of the *Epha2*-null lens was also significantly less than wild-type consistent with early lens growth inhibition.

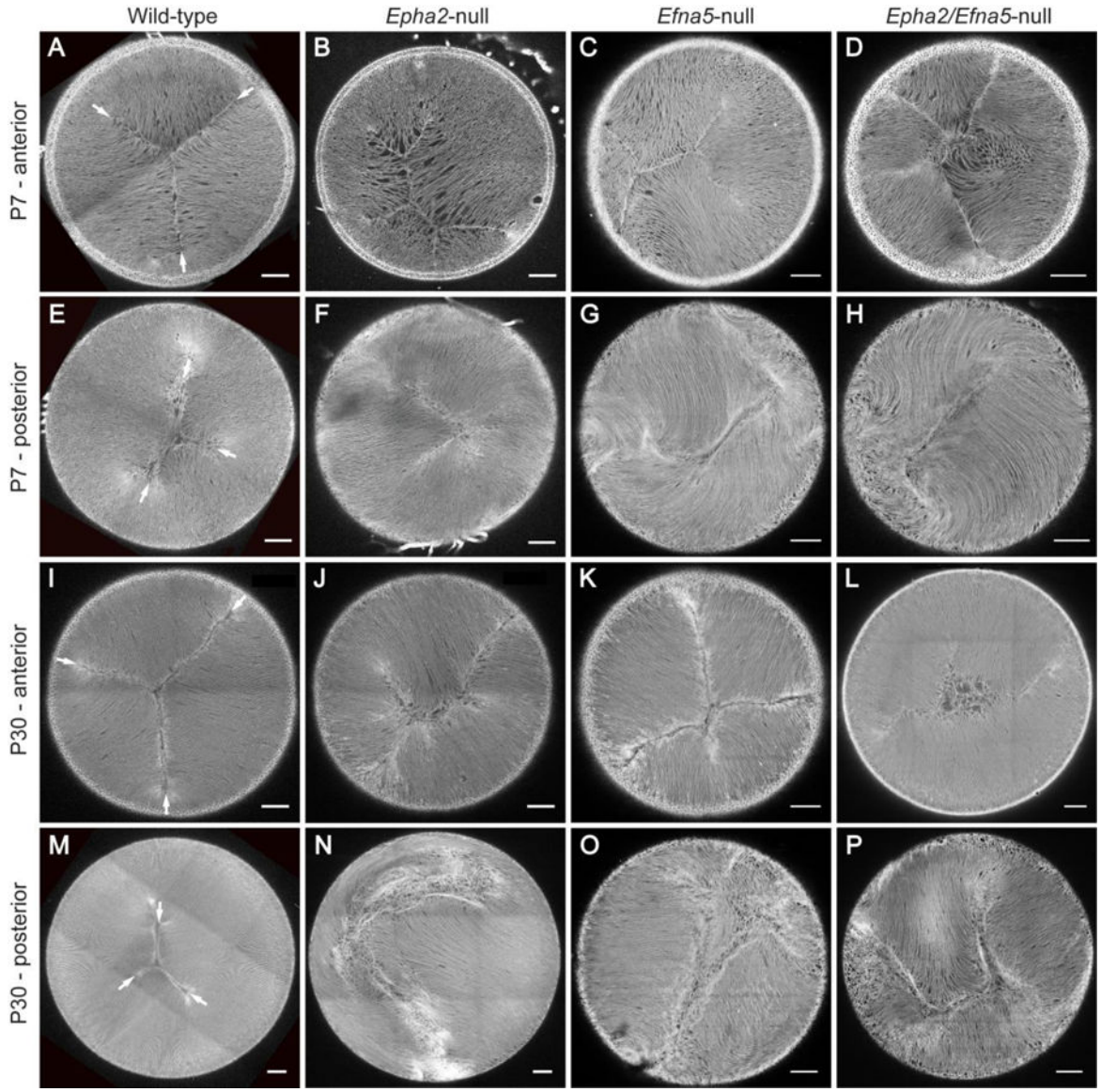

Fig. 4.

Ex vivo imaging of Y-suture formation in tdT labelled mouse lenses. (**A-D, I-L**) Anteriorpole view of the wild-type-tdT (**A, I**), *Epha2-null*-tdT (**B, J**), *Efna5-null*-tdT (**C, K**), and *Epha2/Efna5*-null-tdT (**D, L**) lenses showing grossly disturbed formation (**B-D, J-L**) of the upright Y-suture pattern (arrows) found in wild-type (**A, I**) at P7 (**A-D**) and P30 (**I-L**). (**E-H, M-P**) Posterior-pole view of the wild-type-tdT (**E, M**), *Epha2-null*-tdT (**F, N**), *Efna5-null*-tdT (**G, O**), and *Epha2/Efna5*-null-tdT (**H, P**) lenses showing variably and progressively disturbed formation (**FH, N-P**) of the inverted Y-suture pattern (arrows) found in wild-type (**E, M**) at P7 (**E-H**) and P30 (**M-P**). Image depth from lens surface: 100 – 150 μm (A-D, E, G, I-L, M), 100 – 50 μm (F, H, N). Scale bar: 100 μm. (n = 80, 76, 24, and 8 for wild-type, *Epha2*-null, *Efna5*-null, and *Epha2/Efna5*-null lenses, respectively, with representative images shown).

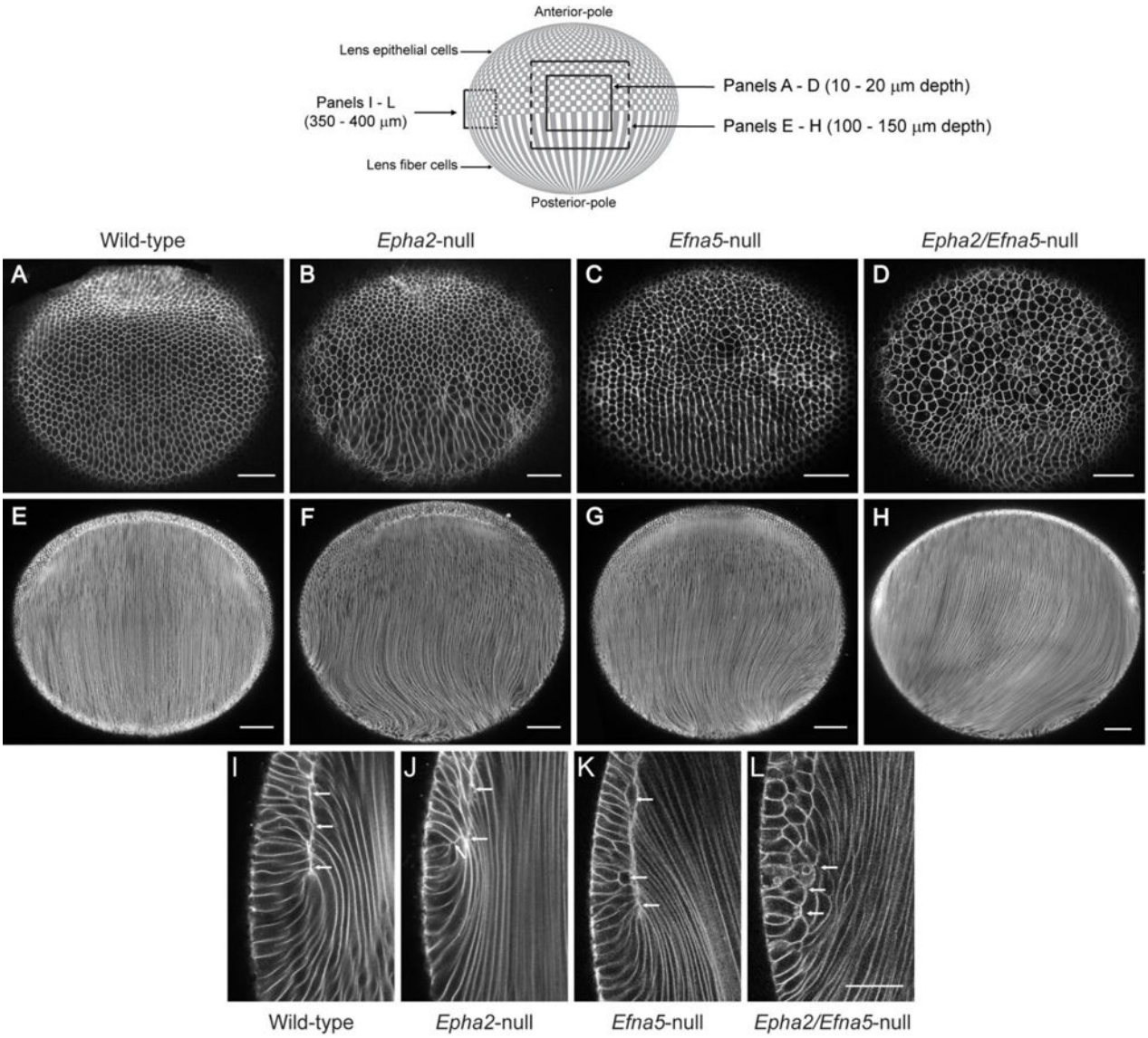

Fig. 5.

Ex vivo imaging of epithelial-to-fiber cell alignment in tdT labelled mouse lenses. A schematic of the mouse lens (equatorial view) is shown above the figure to indicate the confocal microscope imaging planes at various depths from the lens surface shown in panels AL below. (Solid lines lie at the lens surface. Dotted lines lie within the lens mass). (**A-D**) Superficial equatorial view (10 – 20 um depth) of the wild-type-tdT lens (**A**), *Epha2-null*-tdT lens (**B**), *Efna5-null*-tdT lens (**C**), and *Epha2/Efna5*-null-tdT lens (**D**) at P7 showing misalignment of fiber cell meridional rows (B-D). (**E-H**) Intermediate equatorial view (100 – 150 μm depth) of the wild-type-tdT lens (**E**), *Epha2-null*-tdT lens (**F**), *Efna5-null*-tdT lens (**G**), and *Epha2/Efna5*-nulltdT lens (**H**) at P7 showing mistargeting of fiber cells to the poles, particularly the posterior pole (D, F, H). (**I-L**) Deep equatorial view (350 – 400 μm depth) of the wild-type-tdT lens (**I**), *Epha2null*-tdT lens (**J**), *Efna5-null*-tdT lens (**K**), and *Epha2/Efna5*-null-tdT lens (**L**) at P7 showing that the fulcrum interface between the apical

ends of epithelial and fiber cells was disturbed (J-L, arrows) compared with wild-type (I, arrows). Scale bar: 50 μm (**A-D, I-L**), 100 μm (**E-H**). (n = 24, 26, 16, and 4 for wild-type, *Epha2*-null, *Efna5*-null, and *Epha2/Efna5*-null lenses, respectively, with representative images shown).

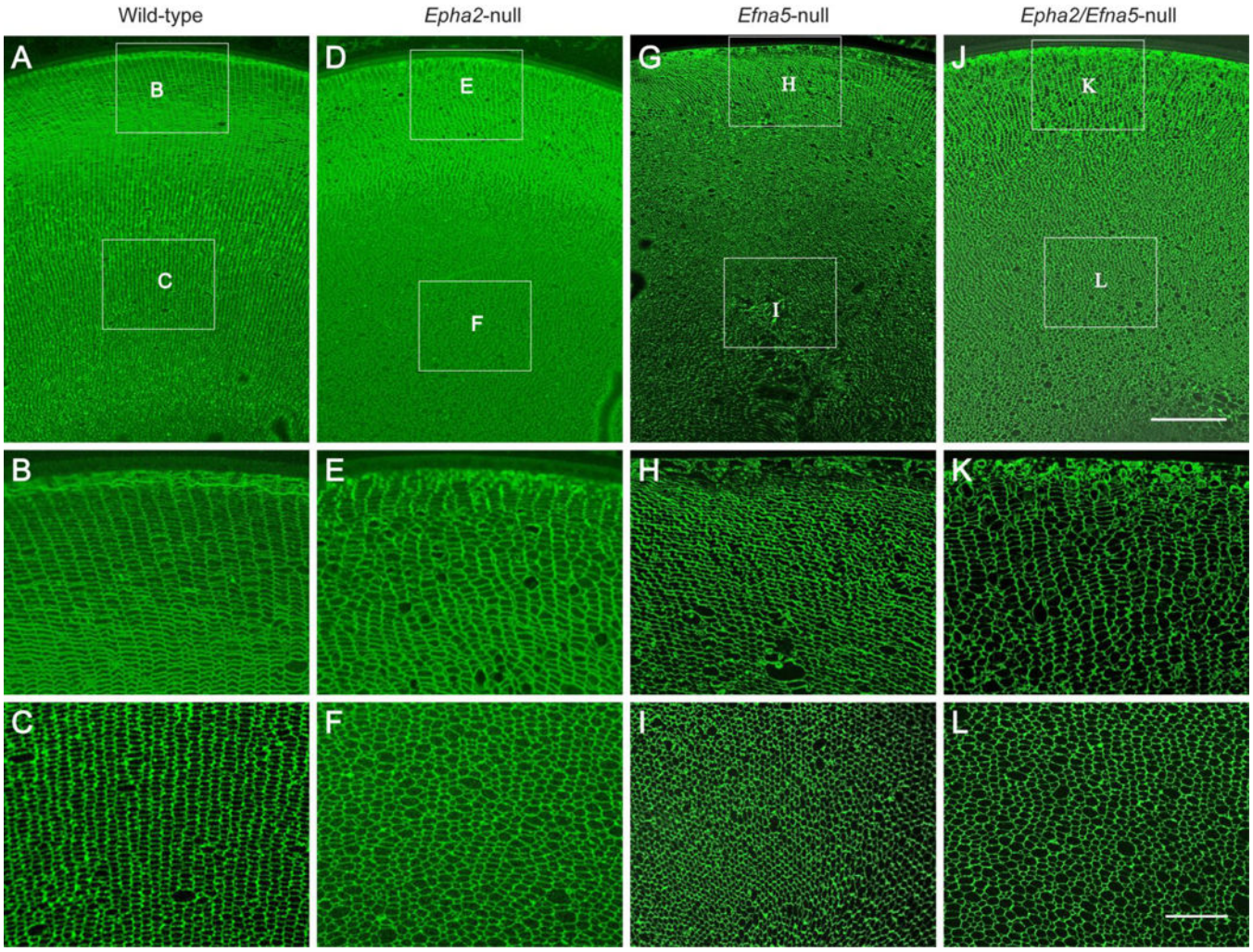

Fig. 6.

Immuno-localization of AQP0 in mouse lens sections (P30). Coronal section (crossoptical plane) view of the wild-type lens (**A-C**), *Epha2*-null lens (**D-F**), *Efna5*-null lens (**G-I**), and *Epha2/Efna5*-null lens (**J-L**) at P30 labeled with AQP0 antibody. Note that the radial columns of hexagonal fiber cells in the outer cortex (**B**) and inner cortex (**C**) of the wild-type lens are variably disturbed in the outer and inner cortex regions of the *Epha2*-null lens (**E, F**), *Efna5*-null lens (**H, I**), and *Epha2/Efna5*-null lens (**K, L**). Scale bar: 100 μm (**A, D, G, J**), 30 μm (**B, C, E, F, H, I, K, L**).